Design of MW-Class Coaxial Gyrotron Cavities With Mode-Converting Corrugation Operating at the Second Cyclotron Harmonic

Dimitrios V. Peponis, Konstantinos A. Avramidis, Ioannis G. Chelis,
Zisis C. Ioannidis, *Member, IEEE*, Stefan Illy, John Jelonnek, *Senior Member, IEEE*,
George P. Latsas, and Ioannis G. Tigelis, *Senior Member, IEEE*

Abstract—This article presents investigations on the design of coaxial gyrotron cavities with mode-converting corrugations, operating at the second harmonic of the electron cyclotron frequency with output power of the order of megawatts. The suppression of the competing modes interacting at the fundamental cyclotron frequency is achieved by the combination of a corrugated coaxial insert and mode-converting corrugation on the outer wall. The outer corrugation couples the key competing modes to lower order modes with reduced quality factor. The design steps, which form a generally applicable design procedure, are described in detail. As an illustrative example, the proposed procedure is used for the design of a cavity for a fusion-relevant, second-harmonic MW-class gyrotron, operating at 170 GHz with the $TE_{37,18}$ mode. From the simulations, it is found that for the proposed design, this mode is excited with an output power of around/$\sim$1.5 MW. Two additional paths for cavity optimization toward even higher output power are also presented.

Index Terms—Coaxial cavities, gyrotron, mode-converting corrugation, second harmonic.

I. INTRODUCTION

IN MODERN fusion experiments, there is a strong requirement for high-power, continuous-wave (CW) electromagnetic radiation sources in the megawatt range with the frequency at the range of $\sim$100–200 GHz (or may be even higher in the near future) [1], [2]. The most appropriate source providing such coherent radiation is the gyrotron oscillator [3], where an electron beam transfers part of its kinetic energy to the electromagnetic field via the Electron Cyclotron Maser Instability (ECMI) mechanism. The gyrotron resonators, called cavities, are either hollow or coaxial, where, in the latter case, there is usually a large number of small surface impedance corrugations engraved on the coaxial conductive insert, in order to enhance the mode selectivity of the resonator [4], [5].

The gyrotrons operate at a frequency f, which is close to the electron cyclotron frequency, multiplied by the integer harmonic number s ($s = 1$ for beam–wave interaction at the fundamental cyclotron frequency)

$$f \approx \frac{s}{2\pi} \frac{eB}{\gamma m_e} \qquad (1)$$

where e is the electron charge, B is the magnetostatic field, γ is the relativistic factor, and m_e is the electron rest mass. As the frequency requirements increase, there is a consequent increase of the magnetostatic field, which is provided by a complex magnet comprising several superconducting coils. Such an increase of the magnetostatic field results in an increase in the cost of the magnet itself as well as in various manufacturing challenges. This requirement can be mitigated by operating the gyrotron at the second cyclotron harmonic [$s = 2$ in (1)], where the magnetostatic field is reduced by half compared to that in the first-harmonic operation [6].

The CW second-harmonic operation of a gyrotron tube has gained ground in dynamic nuclear polarization (DNP) applications, where sub-THz radiation is required, at power levels of hundreds of watts [7], [8], [9]. The second-harmonic operation of gyrotrons has been also studied for fusion applications, but at lower frequencies and output power in the range of a few hundred kilowatts [10]. In addition, the excitation of high-order modes at 340 GHz with output power of the order of 100 kW CW has been theoretically demonstrated [11], and,

more recently, second-harmonic operation at 60 GHz with output power at the level of hundreds of kilowatt has been investigated [12]. Regarding megawatt-level second-harmonic operation, the possibility of employing the injection locking concept, where an external signal is injected in the cavity to "lock" the operating mode and favor its excitation, has been theoretically studied in [13]. The injection locking concept seems promising for second-harmonic operation and has been experimentally demonstrated for short-pulse first-harmonic operation recently [14], however requiring an auxiliary gyrotron driving the main tube, thus increasing the complexity and the overall cost of the necessary infrastructure. As a less complex alternative concept for MW-class second harmonic operation, we propose in the present article the use of coaxial cavities with surface impedance corrugation on the insert as well as mode-converting corrugation on the outer wall.

When it is required for the operating mode to interact with the electron beam at the second cyclotron harmonic, strong mode competition from modes interacting at the first harmonic is expected to take place since the first-harmonic interaction is stronger than the second-harmonic one [1]. The competition becomes significantly severe for MW-class operation because the order of the second-harmonic operating mode must be quite high and, consequently, the number of modes in resonance with the beam becomes larger. Therefore, one should arrive at a situation where the dangerous first-harmonic competitors are suppressed, and the second-harmonic operating mode is left unaffected. It has been shown in [11] and [15] that this can be achieved by coaxial cavities with appropriately designed coaxial inserts and further elaborated in [16] and [17], focusing on CW MW-class second-harmonic operation.

Further enhancement of the mode selectivity at the second harmonic can be achieved by properly rearranging the eigenvalue spectrum of the modes in a way that the first-harmonic competitors are coupled with low-order modes with low quality factor and the operating mode is left uncoupled. The coupling with low-quality-factor modes prevents the excitation of these modes and eventually suppresses them. This way of suppression of the first-harmonic competitors can be achieved by introducing azimuthal corrugation on the cavity's outer wall, with geometrical characteristics chosen accordingly for the appropriate coupling to be introduced. This concept was proposed in [18], where it was used in a coaxial gyrotron cavity for enhancing the operation of a first-harmonic gyrotron and was adopted in [19]. It was also used in [20], albeit without a coaxial insert, for low-power second-harmonic operation at 300 GHz.

In this work, a general systematic method for the design of coaxial gyrotron cavities for MW-class second-harmonic operation is described, where the cavity incorporates surface impedance corrugation on the insert and mode-converting corrugation on the outer wall. The design strategy is illustrated by a cavity design favoring the second-harmonic excitation of the high-order $TE_{37,18}$ mode (eigenvalue $\chi \approx 106$) at 170 GHz with output power larger than 1 MW. The eigenvalue spectra in the corrugated cavity are calculated by using the in-house code 3CI [21], whereas the beam–wave interaction simulations are
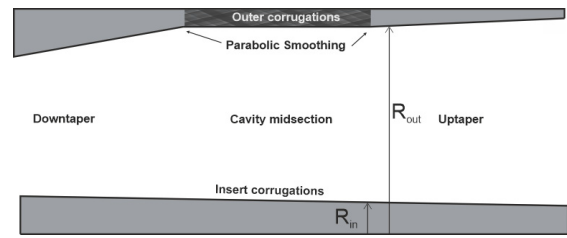

Fig. 1. Axial cross section of the coaxial cavity under investigation.
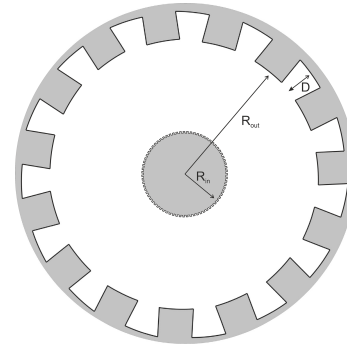

Fig. 2. Transverse cross section of the coaxial cavity with mode-converting corrugations on the outer wall and with surface impedance corrugations on the insert.

performed by the European time-dependent, self-consistent, multimode code EURIDICE [22], which has been upgraded to consider azimuthally coupled modes [23]. The rest of this article is organized as follows. In Section II, the methodology for the cavity design is given in distinct steps, whereas in Section III, the application of this strategy to the design of a cavity for the $TE_{37,18}$ mode is presented. In Section IV, further optimization of the operation of the designed cavity is performed. In Section V, this work is concluded with discussion of the results.

II. DESIGN METHODOLOGY

We describe in discrete steps the procedure toward the design of a coaxial gyrotron cavity with surface impedance corrugation on the insert and with mode-converting corrugation on the outer wall for achieving MW-class operation at the second cyclotron harmonic. A typical schematic of such a cavity is given in Figs. 1 and 2. The design steps are presented as follows.

A. Selection of an Initial Cavity Design

An initial coaxial cavity design with smooth outer wall and surface impedance corrugation on the insert must be obtained as a first step, considering only the operating mode and neglecting mode competition. For a given operating frequency and power level, the selection of the operating mode and the geometrical properties of the smooth outer wall and coaxial insert is performed, based on the standard considerations for hollow cavity designs, observing several constraints (e.g., ohmic wall loading) [24], [25].

With respect to the coaxial insert, the strategy proposed in [11] is used, i.e., the insert is downtapered with corrugation depth around 0.4 λ_0, where λ_0 is the free-space wavelength at the operating frequency. The number of the inner corrugations

N should be related to the azimuthal index of the operating mode m following the SIM criterion [26]:

$$N \gg 2m \tag{2}$$

to avoid coupling of the operating mode with low-order modes due to the insert corrugation.

For simplicity, the operating mode will be denoted as $\text{TE}_{m\text{op},p\text{op}}$ for the rest of this article. Considering that the magnetostatic field value is about half of that required for first-harmonic operation, a preliminary operating point is derived, with methodologies similar to [27], [28], and [29].

B. Identification of the Competing Modes

Self-consistent startup simulations considering only the second-harmonic competing modes are performed. The results of such simulations indicate the beam kinetic energy E_b range at which the operating mode is excited. Then, a self-consistent, time-dependent startup simulation is performed considering both the first- and second-harmonic competing modes, indicating which of the first-harmonic competing modes is possibly the most dangerous one and prevents the operating mode from being excited. This mode ($\text{TE}_{mc,pc}$) appears in the same E_b range as the operating one and should be suppressed.

C. Suppression of the First-Harmonic Competing Mode

The suppression of the first-harmonic competitor is achieved by coupling it with a lower order mode induced due to the introduction of azimuthally periodic mode-converting corrugation on the outer wall [21]. This coupling results in a significant decrease of the diffractive quality factor of the mode and in its consequent elimination.

The mode-converting corrugation properties are derived by initially considering the cavity with corrugation only on the insert. Note that, an eigenvalue curve depicts the root of the characteristic equation of a mode versus the C ratio of the outer wall radius over the insert radius ($C = R_{\text{out}}/R_{\text{in}}$). The coupling of two modes can be roughly expected in zero-order approximation at the intersection of their eigenvalue curves [21], provided that the spatial harmonic method (SHM) criterion holds for those two modes. This criterion relates the azimuthal indices of the coupled mode to the number of the corrugations and arises naturally from the application of the Floquet theorem to the solution of the electromagnetic problem in the transverse cross section of a coaxial waveguide with azimuthal corrugation on the outer wall [26], foreseeing foresees that, in a cavity with M outer corrugations, a mode with azimuthal index m is coupled to a mode with azimuthal index m_c if and only if

$$m_c = m \pm qM \tag{3}$$

where the integer q is the so-called azimuthal harmonic index. By investigating a number of combinations of q and M, we identify an appropriate M, which introduces in the eigenvalue spectrum a lower order mode with azimuthal index $m_{c,1}$ that is coupled with the critical first-harmonic competing mode $\text{TE}_{mc,pc}$ at the C-range corresponding to the cavity midsection. In addition, it should be ensured that

lower order modes are not coupled with the operating mode $\text{TE}_{m\text{op},p\text{op}}$ in the same C-range.

D. Incorporation of Outer Corrugation

Next, the M mode-converting outer corrugations are introduced on the outer wall, and the selection of M is further validated by calculating the eigenvalue curves and the mode coupling in the upgraded cavity by the numerical code 3CI. To restrict the mode coupling only at the cavity midsection and avoid any undesired mode conversion toward the uptaper (including conversion of the operating mode as well), the outer corrugation is localized at the midsection. In addition, to avoid possible undesired mode conversion at the ends of the corrugated region, the transition from/to the corrugated region is not performed abruptly, i.e., the depth of the corrugation is adjusted smoothly, following a sigmoidal profile along the z-axis. The eigenvalue curves are then imported in EURIDICE, where the multimode self-consistent simulations are performed.

III. Illustrative Example of Cavity Design
A. Application of Design Steps

To illustrate the above presented methodology, we applied it to the design of an MW-class coaxial cavity operating with the $\text{TE}_{37,18}$ mode (eigenvalue $\chi = 105.8$ and relative caustic radius $R_c = m/\chi_{mp} = R_{37,18} = 0.35$) at 170 GHz and at the second cyclotron harmonic. The design is inspired by the existing 170 GHz–2 MW coaxial-cavity gyrotron at KIT [29], operating with the $\text{TE}_{34,19}$ mode ($\chi = 105.2$ and $R_{34,19} = 0.32$) at the first harmonic. The reason for not choosing $\text{TE}_{34,19}$ in this illustrative, yet realistic, example was the fact that numerical results [16] indicate that second-harmonic MW-class operation with this mode may be possible even without the use of outer wall corrugation. It should be noted that the selection of $\text{TE}_{37,18}$ as the operating mode is to some extent arbitrary, to demonstrate the generality of the method. Our mode-selection criteria demand only: 1) an eigenvalue similar to that of $\text{TE}_{34,19}$, in order to be compatible with 2 MW CW operation at 170 GHz and 2) a relative caustic radius similar to that of $\text{TE}_{34,19}$, so that a possible future implementation of our design could be combined with an electron gun similar to that used in existing European gyrotrons.

For operation with the $\text{TE}_{37,18}$ at 170 GHz, the cavity radius should be $R_{\text{out}} = 29.86$ mm, and the midsection length is chosen to be 22 mm for efficient interaction at the second cyclotron harmonic. The depth of the insert corrugation is $d \approx 0.4\lambda_0 = 0.71$ mm, according to the previous discussion. By performing cold-structure calculations, it has been found that, to keep the ohmic loading on the coaxial insert below 0.2 kW/cm^2, the radius R_{in} should be 8.58 mm (Table I). Furthermore, the coaxial insert incorporates $N = 75$ surface impedance corrugations.

According to the presented design steps, the list of competing modes at the first and the second harmonic is derived for the initial coaxial cavity without outer corrugation. In our modeling, we consider only the most dangerous modes (in both harmonics) among those whose relative beam coupling

TABLE I
CAVITY GEOMETRICAL PROPERTIES

Quantity	Value
Insert tapering angle (degrees)	-1
Downtaper angle θ_d (degrees)	10
Uptaper angle θ_u (degrees)	2.5
Uptaper smoothing length (mm)	2
Cavity radius at midsection R_{out} (mm)	29.69
Insert radius at the start of midsection R_{in} (mm)	8.58
Downtaper length L_d (mm)	19
Midsection length L_m (mm)	22
Uptaper length L_u (mm)	27

TABLE II
CONSIDERED MODES IN SIMULATIONS

Cyclotron Harmonic s	Modes
1	TE$_{12,12}$, TE$_{16,10}$, TE$_{17,10}$, TE$_{18,09}$, TE$_{18,10}$, TE$_{19,10}$
2	TE$_{-32,19}$, TE$_{-33,20}$, TE$_{-33,21}$, TE$_{36,18}$, TE$_{37,18}$

TABLE III
ELECTRON BEAM PROPERTIES

Quantity	Value
Beam energy E_b (keV)	90
Beam current I_b (A)	75
Pitch angle α	1.3
Pitch angle RMS spread $\delta\alpha$	5%
Kinetic energy RMS spread δE_{kin}	0.1%

is larger than 70% compared to that of the operating mode, and their reduced eigenvalues are in the range of 95%–105% of the eigenvalue of TE$_{37,18}$ ($\sim$105, second-harmonic competing modes) and half of it ($\sim$52, first-harmonic competitors). The considered modes are given in Table II.

Next, a multimode interaction simulation is performed. The beam radius is set equal to the radial position where the coupling factor of TE$_{37,18}$ is maximized, i.e., $R_b = 10.55$ mm. The rest of the beam properties are given in Table III. The magnetostatic field profile is realistic and similar to that used in the KIT coaxial-cavity gyrotron, whereas its maximum value has been chosen in order for the starting current of TE$_{37,18}$ to be minimum, considering beam kinetic energy $E_b = 90$ keV. Moreover, the electron beam is characterized by typical spreads in electron velocity ratio α (pitch angle) and E_b, the values of which are also given in Table III.

The resonance range of TE$_{37,18}$ with this beam configuration has been obtained by a single-mode interaction simulation, the results of which are given in Fig. 3. The multimode interaction results of a typical diode startup scenario are given in Fig. 4. It is clear that TE$_{37,18}$ is not excited in the multimode environment, and the mode sequence includes only the first-harmonic modes with eigenvalues $\chi \approx 52$. Considering the multimode results, it seems that TE$_{17,10}$ prevents primarily the excitation of TE$_{37,18}$ since it appears in the same E_b range during the startup. Therefore, TE$_{17,10}$ should be suppressed by introducing mode-converting corrugation on the outer wall.
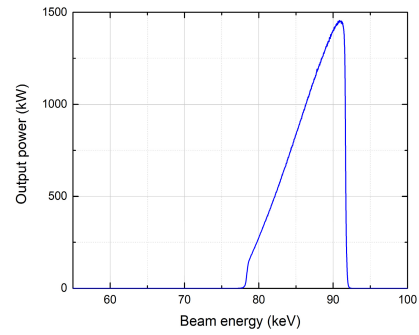

Fig. 3. Single-mode simulation results of TE$_{37,18}$ in the cavity with inner corrugations only.
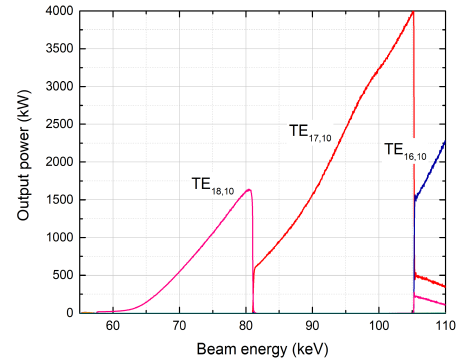

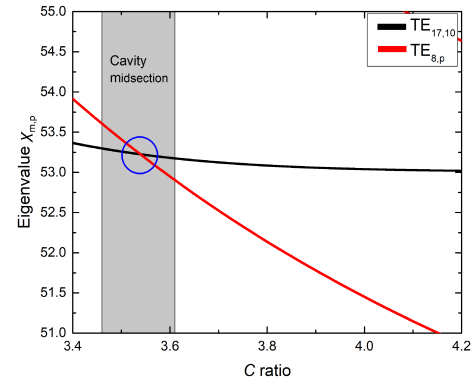Fig. 4. Multimode simulation results of the initial cavity with inner corrugations only.

Fig. 5. Eigenvalue curve of TE$_{17,10}$ versus C-ratio in the absence of outer corrugation. The curve of TE$_{8,p}$ is also shown. Encircled areas depict possible coupling if $M = 25$ outer corrugations are introduced.

It has been found that, by introducing $M = 25$ outer corrugations, TE$_{17,10}$ is coupled with TE$_{8,p}$ in the C-range $C = 3.46$–3.61, which corresponds to the midsection of the cavity. Meanwhile, TE$_{37,18}$ remains uncoupled in the same C-range. Indeed, the eigenvalue curves of these modes in the absence of outer corrugations are given in Fig. 5 (for TE$_{17,10}$) and in Fig. 6 (for TE$_{37,18}$), where it is clearly seen that the curve of TE$_{8,p}$ intersects that of TE$_{17,10}$ (and therefore coupling is expected to take place there), whereas TE$_{37,18}$ is unaffected in this specific C-range. The depth of the outer corrugation D is chosen at 0.1 mm, which has been shown to provide a good balance between the diffractive Q factor and the ohmic Q factor of the operating mode [19].
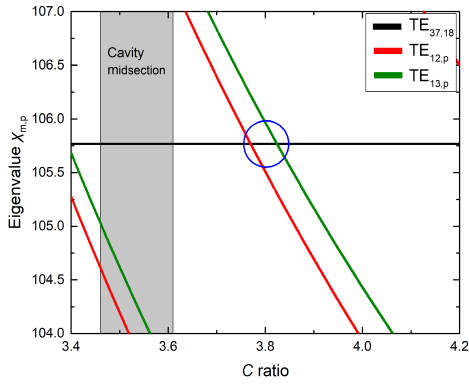
Fig. 6. Eigenvalue curve of $TE_{37,18}$ versus C-ratio in the absence of outer corrugation. The curves of $TE_{12,p}$ and $TE_{13,p}$ are also depicted. Encircled areas depict possible coupling if $M = 25$ outer corrugations are introduced.
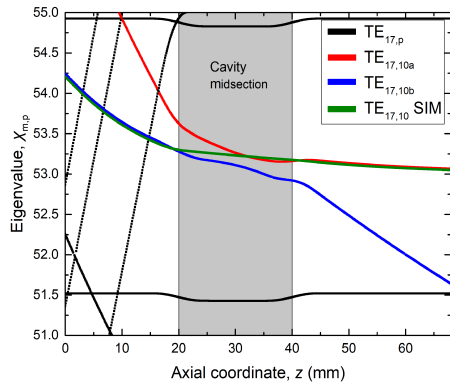

Fig. 7. Eigenvalue curve of $TE_{17,10}$ versus C-ratio considering $M = 25$. The curves of $TE_{8,p}$ are also shown.
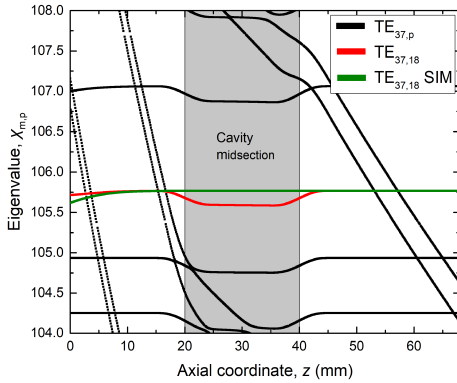

Fig. 8. Eigenvalue curve of $TE_{37,18}$ versus C- ratio considering $M = 25$. The curves of $TE_{12,p}$ and $TE_{13,p}$ are also depicted.

The eigenvalue curves versus the axial coordinate z of the cavity, including the outer corrugation (cavity UpA), are given in Fig. 7 for $TE_{17,p}$ and in Fig. 8 for $TE_{37,p}$. In the same figure, the eigenvalues considering corrugation only on the insert are also given, calculated by the surface impedance model (SIM) [4]. It is evident that $TE_{17,10}$ is altered and divided into two coupled branches [19], [21], $TE_{17,10a}$ and $TE_{17,10b}$, in the midsection (denoted by the shaded rectangle in the figures), whereas $TE_{37,18}$ is left almost unaffected, with a "dip" in the midsection due to the presence of the outer

TABLE IV
DIFFRACTIVE QUALITY FACTORS FOR THE CAVITIES UNDER INVESTIGATION

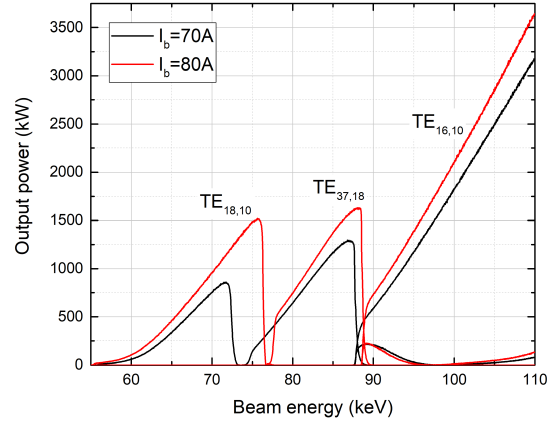| Mode	Cavity	Q
$TE_{37,18}$	Initial	2845
$TE_{37,18}$	UpA	4119
$TE_{17,10}$	Initial	452
$TE_{17,10a}$	UpA	268
$TE_{17,10b}$	UpA	234

Fig. 9. Multimode simulation results of the cavity UpA with both inner and outer corrugations and $D = 0.1$ mm.
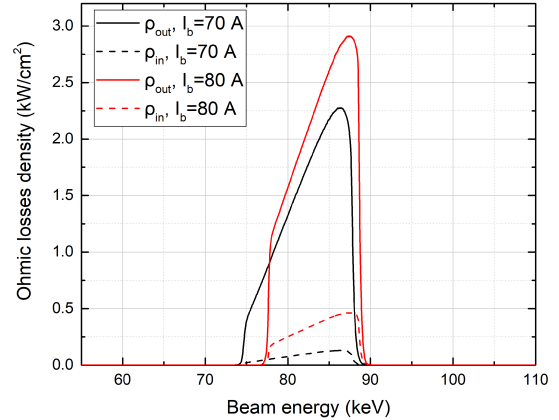

Fig. 10. Ohmic loading of the inner rod and outer conducting wall of cavity UpA.

corrugation in that region. The Q factors of these modes in the two cavities (without and with outer corrugation) are given in Table IV, where it is evident that the Q factor of $TE_{37,18}$ increases, whereas the corresponding values of the branches of $TE_{17,10}$ decrease. Therefore, it is expected that $TE_{37,18}$ will be excited, whereas $TE_{17,10}$ will be altered and transformed, and eventually suppressed.

B. Interaction Results of the Upgraded Cavity

The beam properties that have been used in the simulations of the upgraded cavity with outer wall corrugation are the same as in the simulations of the structure without the outer corrugation (Table II). Parametric multimode simulations with respect to the beam current were performed for the upgraded cavity with outer-wall corrugation. It was found that $TE_{37,18}$ is excited and is stable for $I_b \leq 80$ A. The output power for

TABLE V
QUALITY FACTORS OF THE CONSIDERED CAVITY DESIGNS

Cavity	D (mm)	l_s (mm)	Q
UpA	0.1	2.0	4119
UpB	0.05	2.0	3370
UpC	0.1	4.5	2503

$I_b = 70$ A and $I_b = 80$ A is given in Fig. 9, whereas in Fig. 10, the ohmic loading of the inner rod and outer wall for the same values of I_b is presented. The maximum power for $I_b = 80$ A is 1.7 MW with 24% interaction efficiency. However, as it can be seen from Fig. 10, the ohmic loading is exceeding the technological constraints proposed in [30], which are $\rho_{\text{out,max}} = 2.2$ kW/cm^2 for the outer wall and $\rho_{\text{in,max}} = 0.39$ kW/cm^2 for the coaxial insert. (Note that, in our simulations, the effective conductivity of the walls has been set equal to $\sigma = 1.73 \times 10^7$ S/m, to account both for the increased wall temperature in CW operation and the surface roughness. This results in a correction factor of $\sim$1.8 in the calculation of the ohmic loading, with respect to the case of walls from ideal smooth copper at room temperature.) In order to comply to the ohmic loading constraints of [30], a current $I_b = 70$ A should be used. For this value of I_b, the maximum output power of TE$_{37,18}$ is 1.3 MW at 22% interaction efficiency. It can also be seen that the first-harmonic competitors TE$_{16,10}$ and TE$_{18,10}$ are also excited for both values of the current. However, a beam kinetic energy range of stable excitation of TE$_{37,18}$ is secured and the main competitor TE$_{17,10}$ is successfully suppressed. Therefore, the introduction of outer corrugation significantly enhances this cavity design allowing the excitation of the mode of interest TE$_{37,18}$, which otherwise is not excited without the outer corrugation.

It is clear from the simulation results that the increased ohmic loading (ohmic loss density) limits the output power and efficiency, if the constraints of [30] are to be met. The higher ohmic loading is due to the increased Q factor of the structure, which in turn is due to the "dip" of the eigenvalue curve of TE$_{37,18}$ (see Fig. 8). To increase I_b without exceeding the ohmic loading limits, the Q factor of the cavity should be decreased. This can be achieved by decreasing the outer corrugation depth D (and consequently the eigenvalue "dip") or by increasing the outer wall smoothing length l_s between the midsection and the uptaper. These approaches are investigated in the following section.

IV. OPTIMIZATION OF THE CAVITY PERFORMANCE

A. Decrease of Outer Corrugation's Depth

The depth of the outer corrugation D was reduced to 0.05 mm while keeping the smoothing length l_s the same as previously. The Q factor of TE$_{37,18}$ in this cavity (UpB) is significantly decreased compared to the cavity UpA (Table V). It has been found that I_b can now be increased up to 85 A, whereas the ohmic loading is below the constraints described previously. For this value of I_b, the maximum output power of TE$_{37,18}$ is 1.55 MW, at 22% interaction efficiency. For larger values of I_b, TE$_{37,18}$ is not excited due to mode competition.

TABLE VI
SUMMARY OF RESULTS FOR THE CONSIDERED CASES

Cavity	Q	E_b (keV)	I_b (A)	P_{out} (MW)	η (%)	ρ_{out} (kW/cm^2)	ρ_{in} (kW/cm^2)
UpA	4119	90	70.0	1.30	22.0	2.21	0.35
UpB	3370	90	85.0	1.55	22.5	2.13	0.06
UpB	3370	110	65.0	1.50	21.0	2.20	0.06
UpB	3370	110	74.5	1.90	23.5	2.82	0.06
UpC	2503	90	85.0	0.97	15.0	0.97	0.09
UpC	2503	130	80.0	1.95	20.0	2.19	0.20

Single-mode parametric studies indicated that increased output power can also be achieved, if the beam power is increased up to 8.8 MW by increasing the beam kinetic energy while keeping I_b low, to avoid strengthening the mode competition. Of course, since the operating point changes (hereafter, it is called high-voltage operating point, HVOP), the optimum value of the magnetostatic field was recalculated and was set to $B = 3.58$ T. Parametric multimode simulations with I_b showed that, at beam kinetic energy $E_b = 110$ keV, the maximum power achieved, while keeping the ohmic loading within the aforementioned constraints, is $P_{\max} = 1.5$ MW for $I_b = 65$ A at 21% interaction efficiency. Note that TE$_{37,18}$ is stable up to $I_b = 74.5$ A, where $P_{\max} = 1.9$ MW at 23.5% interaction efficiency, but with $\rho_{out} = 2.82$ kW/cm^2 and $\rho_{in} = 0.062$ kW/cm^2.

B. Increase of Midsection/Uptaper Smoothing Length

An alternative method of decreasing the Q factor is by increasing the smoothing length between the midsection and the uptaper l_s. In this study, the smoothing length of the uptaper is increased from $l_s = 2$ mm to $l_s = 4.5$ mm while keeping $D = 0.1$ mm for the outer corrugation. The Q factor of this cavity (UpC) is significantly reduced compared to the initial cavity design, UpA (Table V). As previously, a parametric multimode study with respect to I_b has been performed considering $E_b = 90$ kV, the results of which showed a maximum power $P_{\max} = 0.97$ MW for $I_b = 85$ A. For larger values of I_b, TE$_{37,18}$ is not excited due to mode competition, which has been strengthened because of the decreased Q factor of the operating mode. An HVOP has been investigated ($E_b = 130$ kV, $I_b = 80$ A, and $B_{\max} = 3.675$ T) where $P_{\max} = 1.95$ MW with 20% interaction efficiency. It is clear that the output power has been significantly increased at the expense of somewhat decreased efficiency, as expected in cases with high E_b. In Table VI, a summary of the previous results is presented with the corresponding ohmic loading values.

V. CONCLUSION

In this work, a design methodology for coaxial cavities with outer corrugation targeting second-harmonic MW-class CW operation has been presented. Generally applicable design steps have been described in detail. It is shown that, by introducing a properly selected number of corrugations on the outer cavity wall, the selected operating mode can be excited and the severe competition from first- and second-harmonic competing modes is mitigated.

The design strategy has been applied to the indicative case of the excitation of the $TE_{37,18}$ mode at 170 GHz at the second cyclotron harmonic, with output power over 1 MW. It is demonstrated that the introduction of outer corrugation leads to the excitation of $TE_{37,18}$, which otherwise is not excited in a cavity with smooth outer wall. Further enhancement of the illustrative case has been performed, where the output power has been increased significantly, reaching the vicinity of 2 MW.

The proposed design procedure constitutes an important tool for the design of efficient MW-class CW coaxial gyrotron cavities operating at the second cyclotron harmonic. Compared to the method of elimination of the first-harmonic competing modes in MW-class second-harmonic gyrotrons proposed in [17], where no outer corrugation is used and a coaxial insert with larger radius is required instead, the ohmic loading of the coaxial insert in the method presented here is quite low. This relaxes significantly the possibly challenging requirements for the insert cooling in CW operation. In addition, the presented method is much less complex compared to that in [13] since no additional gyrotrons are required to provide an external signal for the excitation of the operating second-harmonic mode.

ACKNOWLEDGMENT

REFERENCES

[1] M. V. Kartikeyan, E. Borie, and M. Thumm, *Gyrotrons: High Power Microwave and Millimeter Wave Technology*. Berlin, Germany: Springer, 2004.

[2] M. Thumm, "State-of-the-art of high-power gyro-devices and free electron masers," *J. Infr., Millim., Terahertz Waves*, vol. 41, no. 1, pp. 1–140, Jan. 2020, doi: 10.1007/s10762-019-00631-y.

[3] G. S. Nusinovich, M. K. A. Thumm, and M. I. Petelin, "The gyrotron at 50: Historical overview," *J. Infr., Millim., Terahertz Waves*, vol. 35, no. 4, pp. 325–381, Apr. 2014, doi: 10.1007/s10762-014-0050-7.

[4] C. T. Iatrou, S. Kern, and A. B. Pavelyev, "Coaxial cavities with corrugated inner conductor for gyrotrons," *IEEE Trans. Microw. Theory Techn.*, vol. 44, no. 1, pp. 56–64, Jan. 1996, doi: 10.1109/22.481385.

[5] J. J. Barroso, R. A. Correa, and P. Jose de Castro, "Gyrotron coaxial cylindrical resonators with corrugated inner conductor: Theory and experiment," *IEEE Trans. Microw. Theory Techn.*, vol. 46, no. 9, pp. 1221–1230, Sep. 1998, doi: 10.1109/22.709460.

[6] E. Borie, "Study for second harmonic gyrotrons in the submillimeter region," *Int. J. Infr. Millim. Waves*, vol. 15, no. 2, pp. 311–337, Feb. 1994, doi: 10.1007/BF02096244.

[7] M. V. Kartikeyan, E. Borie, and M. Thumm, "A 250 GHz, 50 W, CW second harmonic gyrotron," *Int. J. Infr. Millim. Waves*, vol. 28, no. 8, pp. 611–619, Aug. 2007, doi: 10.1007/s10762-007-9242-8.

[8] S. K. Jawla, R. G. Griffin, I. A. Mastovsky, M. A. Shapiro, and R. J. Temkin, "Second harmonic 527-GHz gyrotron for DNP-NMR: Design and experimental results," *IEEE Trans. Electron Devices*, vol. 67, no. 1, pp. 328–334, Jan. 2020, doi: 10.1109/TED.2019.2953658.

[9] M. Y. Glyavin et al., "A 250-watts, 0.5-THz continuous-wave second-harmonic gyrotron," *IEEE Electron Device Lett.*, vol. 42, no. 11, pp. 1666–1669, Nov. 2021, doi: 10.1109/LED.2021.3113022.

[10] M. V. Kartikeyan, E. Borie, O. Drumm, S. Illy, B. Piosczyk, and M. Thumm, "Design of a 42-GHz 200-kW gyrotron operating at the second harmonic," *IEEE Trans. Microw. Theory Techn.*, vol. 52, no. 2, pp. 686–692, Feb. 2004, doi: 10.1109/TMTT.2003.822015.

[11] K. A. Avramides, C. T. Iatrou, and J. L. Vomvoridis, "Design considerations for powerful continuous-wave second-cyclotron-harmonic coaxial-cavity gyrotrons," *IEEE Trans. Plasma Sci.*, vol. 32, no. 3, pp. 917–928, Jun. 2004, doi: 10.1109/TPS.2004.828781.

[12] S. Adya, S. Yuvaraj, M. Rawat, M. V. Kartikeyan, and M. K. Thumm, "Investigations on RF behavior of a V-band second harmonic gyrotron for 100/200 kW operation," *IEEE Trans. Plasma Sci.*, vol. 50, no. 2, pp. 222–228, Feb. 2022, doi: 10.1109/TPS.2022.3140350.

[13] G. G. Denisov et al., "Phase-locking of second-harmonic gyrotrons for providing MW-level output power," *IEEE Trans. Electron Devices*, vol. 69, no. 2, pp. 754–758, Feb. 2022, doi: 10.1109/TED.2021.3134187.

[14] A. N. Kuftin et al., "First demonstration of frequency-locked operation of a 170 GHz/1 MW gyrotron," *IEEE Electron Device Lett.*, vol. 44, no. 9, pp. 1563–1566, Sep. 2023, doi: 10.1109/LED.2023.3294755.

[15] V. I. Shcherbinin, "Multifunctional coaxial insert with distributed impedance corrugations for cavities of broadband tunable second-harmonic gyrotrons," *IEEE Trans. Electron Devices*, vol. 68, no. 8, pp. 4104–4109, Aug. 2021, doi: 10.1109/TED.2021.3090348.

[16] L. Feuerstein, A. Marek, C. Wu, S. Illy, M. Thumm, and J. Jelonnek, "Design of a second harmonic MW-level coaxial gyrotron cavity," in *Proc. 24th Int. Vacuum Electron. Conf.*, Chengdu, China, Apr. 2023, pp. 1–2, doi: 10.1109/IVEC56627.2023.10156958.

[17] I. Chelis et al., "High-frequency MW-class coaxial gyrotron cavities operating at the second cyclotron harmonic," to be published.

[18] V. A. Flyagin et al., "Investigations of advanced coaxial gyrotrons at IAP RAS," *Int. J. Infr. Millim. Waves*, vol. 24, pp. 1–17, Jan. 2003, doi: 10.1023/A:1021667030616.

[19] D. V. Peponis, Z. C. Ioannidis, K. A. Avramidis, and I. G. Tigelis, "Sensitivity analysis of a 140-GHz coaxial gyrotron cavity with corrugations on the inner and outer walls," in *Proc. 41st Int. Conf. Infr., Millim., THz Waves (IRMMW-THz)*, Copenhagen, Denmark, Sep. 2016, pp. 1–2, doi: 10.1109/IRMMW-THz.2016.7758522.

[20] T. Tkachova, V. Shcherbinin, and V. Tkachenko, "Mode-converting corrugations for cavities of second-harmonic gyrotrons with improved performance," *East Eur. J. Phys.*, no. 2, pp. 89–97, Jan. 2021, doi: 10.26565/2312-4334-2021-2-05.

[21] Z. C. Ioannidis, K. A. Avramidis, and I. G. Tigelis, "Selectivity properties of coaxial gyrotron cavities with mode converting corrugations," *IEEE Trans. Electron Devices*, vol. 63, no. 3, pp. 1299–1306, Mar. 2016, doi: 10.1109/TED.2016.2518217.

[22] K. A. Avramides, I. G. Pagonakis, C. T. Iatrou, and J. L. Vomvoridis, "EURIDICE: A code-package for gyrotron interaction simulations and cavity design," in *Proc. EPJ Web Conf.*, vol. 32, 2012, p. 04016, doi: 10.1051/epjconf/20123204016.

[23] K. Avramidis, J. Frank, S. Illy, and T. Rzesnicki, "Report on the upgrade of the code-package EURIDICE to address coupled modes," EUROfusion, Garching, Germany, Annu. Rep. HCD-4.2.3-T010-D004, 2017. [Online]. Available: https://idm.euro-fusion.org/default.aspx?uid=2MYHDK

[24] K. E. Kreischer, B. G. Danly, J. B. Schutkeker, and R. J. Temkin, "The design of megawatt gyrotrons," *IEEE Trans. Plasma Sci.*, vol. PS-13, no. 6, pp. 364–373, 1985, doi: 10.1109/TPS.1985.4316447.

[25] K. A. Avramides, C. T. Iatrou, and J. L. Vomvoridis, "Systematic procedure for operating-mode selection in conventional and coaxial-cavity gyrotrons," in *Proc. 14th Joint Workshop Electron Cyclotron Emission Electron Cyclotron Reson. Heating*, Santorini, Greece, May 2006, pp. 484–489.

[26] Z. C. Ioannidis, K. A. Avramidis, G. P. Latsas, and I. G. Tigelis, "Azimuthal mode coupling in coaxial waveguides and cavities with longitudinally corrugated insert," *IEEE Trans. Plasma Sci.*, vol. 39, no. 5, pp. 1213–1221, May 2011, doi: 10.1109/TPS.2011.2118766.

[27] O. Dumbrajs, B. Piosczyk, and C. T. Iatrou, "Mode selection for a 2 MW, CW 170 GHz coaxial cavity gyrotron," in *Proc. 26th Int. Conf. Infrared Millimeter Waves*, Toulouse, France, Sep. 2001, pp. 10–14.

[28] B. Piosczyk et al., "A 2-MW, 170-GHz coaxial cavity gyrotron," *IEEE Trans. Plasma Sci.*, vol. 32, no. 2, pp. 413–417, Apr. 2004, doi: 10.1109/TPS.2004.827605.

[29] S. Ruess et al., "KIT coaxial gyrotron development: From ITER toward DEMO," *Int. J. Microw. Wireless Technol.*, vol. 10, nos. 5–6, pp. 547–555, Jun. 2018, doi: 10.1017/S1759078718000144.

[30] P. C. Kalaria et al., "Multiphysics modeling of insert cooling system for a 170-GHz, 2-MW long-pulse coaxial-cavity gyrotron," *IEEE Trans. Electron Devices*, vol. 66, no. 9, pp. 4008–4015, Sep. 2019, doi: 10.1109/TED.2019.2928222.